Anomalous and Gaussian transport regimes in anisotropic three-dimensional magnetic turbulence

P. Pommois, P. Veltri, and G. Zimbardo
Dipartimento di Fisica, Università della Calabria, I-87030 Arcavacata di Rende, Italy
and Istituto Nazionale di Fisica della Materia, Unità di Cosenza, I-87030 Arcavacata di Rende, Italy
(Received 16 June 1998)

The effects of the anisotropy of magnetic turbulence on the transport of magnetic field lines are investigated numerically. The three-dimensional magnetic turbulence is represented by a Fourier expansion with a power law *band* spectrum, and anisotropy is introduced by considering different correlation lengths l_{cx} and l_{cy} in the plane perpendicular to the average magnetic field $\mathbf{B}_0 = B_0 \hat{e}_z$. Transport in this plane is analyzed for different fluctuation levels $\delta B/B_0$ and for various degrees of anisotropy l_{cx}/l_{cy}. The results of the simulation show that there are anomalous (subdiffusive and superdiffusive) transport regimes at low fluctuation levels, while Gaussian diffusive regimes are attained in the presence of high fluctuation levels, like in the isotropic case; as anisotropy is increased the Gaussian regime is reached for higher fluctuation levels; for significant degrees of anisotropy l_{cx}/l_{cy}, a percolative regime is found at a low fluctuation level, with superdiffusion in the direction where the correlation length is shorter; conversely, in the diffusive regime transport is faster in the direction of the longer correlation length, and the obtained ratio of diffusion coefficients D_x/D_y is close to the ratio of anisotropy l_{cx}/l_{cy}. The application of these results to energetic particle propagation in the solar wind is discussed. [S1063-651X(98)14511-7]

PACS number(s): 52.25.Fi, 02.50.Ey, 95.30.Qd, 05.45.−a

I. INTRODUCTION

Plasma transport across a background magnetic field depends on an understanding of the transport of magnetic field lines in a turbulent magnetic field. Indeed, when the particle velocity is much higher than the phase velocity of waves, plasma particles ''see'' the fluctuations as static. Moreover, when the particle Larmor radii are smaller than the shortest scale lengths of turbulence, particles move along the magnetic field lines. Then magnetic field line diffusion represents one of the main sources of particle transport. This is of fundamental importance for many plasma systems, ranging from fusion confinement devices [1–5] to astrophysical and space plasmas [6–15].

Equations for magnetic field lines form a set of nonlinear differential equations which can be studied by numerical integration. Recently, the authors of Refs. [12] and [15] carried out numerical studies of the magnetic field line transport in a three-dimensional (3D) isotropic turbulence spectrum, pointing out the existence of both Gaussian and non-Gaussian (superdiffusive) transport regimes, the latter implying the occurrence of Lévy flights. In those papers, the distribution of wave mode amplitudes is spherically symmetric. However, the magnetic turbulence found in many physical systems is anisotropic. We expect that this anisotropy influences the way in which the magnetic field line diffuse: The average energy density along each axis will be different, so that transport also should be anisotropic [16]. In addition, the magnetic surfaces are stretched by the anisotropy, and when the level of the magnetic fluctuations is low, the magnetic field lines which are lying in the stochastic layer between the magnetic surfaces are constrained to go around these stretched regions, leading to particular phenomena of transport which need to be investigated.

Indeed, some recent theoretical [5,17–19] and numerical studies [20,14] considered the transport of magnetic field lines with a nearly 2D model of turbulence, which, having all the wave vectors $\mathbf{k}$ in the plane perpendicular to the average magnetic field $\mathbf{B}_0$, corresponds to a very strong anisotropy in $\mathbf{k}$ space.

In particular, magnetohydrodynamic (MHD) turbulence in a solar wind is anisotropic: a first analysis of such anisotropy was performed in Ref. [21], whose authors showed that the $\mathbf{k}$ vectors should be concentrated in the ecliptic plane. More recently, Matthaeus, Goldstein, and Robert [22], analyzed solar wind data to stress the anisotropy of the $\mathbf{k}$ distribution in directions parallel and perpendicular to the average magnetic field. In this analysis they built up a model of turbulence based on the presence of a slab turbulence superposed to a 2D turbulence.

The model of Refs. [18, 14] cannot describe anisotropy in the plane perpendicular to the average magnetic field, since the authors assumed cylindrical symmetry around $\mathbf{B}_0$ from the beginning. Conversely, the analysis of the magnetic perturbation correlation tensor carried out in Ref. [23], based on Helios II observations [24], by assuming different correlation lengths l_{cx}, l_{cy}, and l_{cz} in the x, y, and z directions, respectively, in the expression of the Fourier amplitudes, has shown that in the solar wind the correlation lengths can be very different from each other.

Anisotropy may be due to the geometrical features of the system under consideration [25,26], or to the presence of either a velocity field or a background magnetic field. We argue that the anisotropy found in the solar wind is due to two physical reasons: one is the radial expansion of the solar wind plasma leaving the Sun, and the other is the nonlinear energy cascade of MHD turbulence in the presence of an average magnetic field $\mathbf{B}_0$ [27–31]. The former reasoning

goes as follows: because of the radial expansion of the solar wind, a bubble of plasma is stretched in the transverse directions, and the wave vectors of the magnetic perturbations are squeezed to a ''cigar'' oriented in the radial direction [32]. The same result is obtained if one considers the propagation of MHD waves in a medium with a radially increasing refraction index. The latter cause of anisotropy is related to the so-called Alfvén effect [31], and stems from the fact that nonlinear interactions are much more effective for those wave vectors which are perpendicular to $\mathbf{B}_0$, so that the energy cascade is faster for these wave vectors. Thus the domain of turbulence in $\mathbf{k}$ space tends to be perpendicular to the average field. It is difficult to predict which of these two effects prevails in the solar wind, but it should not be surprising to find different correlation lengths l_{cx}, l_{cy}, and l_{cz}. In the solar wind, we adopt the following coordinate system: x is normal to the $\mathbf{B}_{\mathrm{IMF}}$-$\mathbf{V}_{\mathrm{SW}}$ plane ($\mathbf{B}_{\mathrm{IMF}}$ is the average interplanetary magnetic field and $\mathbf{V}_{\mathrm{SW}}$ is the solar wind speed), z is in the $\mathbf{B}_{\mathrm{IMF}}$ direction, and y completes a right-handed coordinate system. Carbone, Malara, and Veltri [23] found, for a variety of cases, that $l_{cx} \gg l_{cy}, l_{cz}$, implying that the wave vectors are squeezed in the yz plane. Here we would like to investigate a few cases where the anisotropy is in the plane perpendicular to the average magnetic field $\mathbf{B}_0$, and, in a first approach, study what happens when we increase the correlation length l_{cx}.

In a previous paper [15], we performed an accurate study of magnetic field line transport in isotropic turbulence for different types of fully 3D spectrum. It was shown that the ratio between the correlation length l_c and the periodicity scale L influences the features of transport, and that $l_c \ll L$ is needed in order to avoid the dominance of just a few modes. In particular, when using *band* spectrum with both long and short wavelength cutoffs, transport is isotropic and superdiffusive, i.e., anomalous, for low fluctuation levels, $\delta B/B_0 \lesssim 0.1$, and isotropic and diffusive, i.e., Gaussian, for higher fluctuation levels [15]. Since we want to limit the periodicity effects, that are not present in general in astrophysical turbulence, we shall use a *band* spectrum.

In this paper, the transport regimes are analyzed for various fluctuation levels ($\delta B/B_0$), and for different anisotropies by varying the ratio l_{cx}/l_{cy}. As in the isotropic case, we find different regimes of diffusion: an anomalous Lévy flights regime for low $\delta B/B_0$, and a Gaussian regime for high $\delta B/B_0$. The value of fluctuation level $(\delta B/B_0)^*$, where the Gaussian regime is attained, grows as the level of anisotropy l_{cx}/l_{cy} is increased. Also, in the Gaussian regime transport is fastest in the direction x where the correlation length is the largest, and we find that the ratio of the diffusion coefficients D_x/D_y scales as l_{cx}/l_{cy}. At the lower fluctuation levels, we have subdiffusion or superdiffusion regimes. Surprisingly, if the value of l_{cx}/l_{cy} is large enough, the Lévy flights are found mostly in the y direction, where the correlation length is smaller, and they are reinforced when the ratio l_{cx}/l_{cy} is increased.

The plan of this paper is as follows: in Sec. II, we describe the numerical technique, by showing how the anisotropic perturbed magnetic field is modeled. In Sec. III the simulation results are presented: first we give an overview of the Poincaré sections, then the different regimes of transport are analyzed accurately by calculating both the diffusion coefficients and the anomalous diffusion exponents. In Sec. IV we discuss the various results, and consider how they could be applied to the solar wind.

II. NUMERICAL MODEL

A. Numerical technique

A numerical realization of a turbulent magnetic field is set up using a model similar to that of Ref. [15], where we introduced anisotropy by using different correlation lengths l_{cx}, l_{cy}, and l_{cz}. In this model the magnetic field $\mathbf{B}(\mathbf{r})$ at a generic point $\mathbf{r}$ is taken to be the sum of a background field given by $\mathbf{B}_0 = B_0 \mathbf{e}_z$ and of static magnetic perturbations given by

$$\delta\mathbf{B}(\mathbf{r}) = \sum_{\mathbf{k},\sigma} \delta B^{(\sigma)}(\mathbf{k}) \mathbf{e}^{(\sigma)}(\mathbf{k}) \exp\, i[\mathbf{k}\cdot\mathbf{r} + \phi_{\mathbf{k}}^{(\sigma)}]. \qquad (1)$$

Here $\delta B^{(\sigma)}(\mathbf{k})$ is the amplitude of the mode with wave vector $\mathbf{k}$ and polarization σ, ($\sigma = 1$ or 2), $\mathbf{e}^{(\sigma)}(\mathbf{k})$ are the polarization unit vectors, while $\phi_{\mathbf{k}}^{(\sigma)}$ are random phases, chosen to simulate a realization of an ensemble of fluctuating magnetic fields. Having $\nabla \cdot \mathbf{B} = 0$ implies that there are two directions of polarization normal to $\mathbf{k}$, corresponding to the unit vectors

$$\mathbf{e}^{(1)}(\mathbf{k}) = i\, \frac{\mathbf{k}\times\mathbf{B}_0}{|\mathbf{k}\times\mathbf{B}_0|}, \quad \mathbf{e}^{(2)}(\mathbf{k}) = i\, \frac{\mathbf{k}}{|\mathbf{k}|} \times \mathbf{e}^{(1)}(\mathbf{k}), \qquad (2)$$

where $\mathbf{e}^{(1)}(\mathbf{k})$ represents the Alfvénic polarization and $\mathbf{e}^{(2)} \times(\mathbf{k})$ the magnetosonic one. The amplitude is given by the spectrum

$$\delta B^{(\sigma)}(\mathbf{k}) = \frac{A C^{(\sigma)}}{(k_x^2 l_x^2 + k_y^2 l_y^2 + k_z^2 l_z^2 + 1)^{\gamma/4 + 1/2}}, \qquad (3)$$

where A is a normalization constant, $C^{(\sigma)}$ is the weight of each polarization, γ is the spectral index, and $1/l_x, 1/l_y, 1/l_z$ are the rollover wave numbers in the x, y, and z directions. Different Fourier amplitudes $\delta B^{(\sigma)}$ could be given for the Alfvénic and magnetosonic polarizations, for instance by prescribing different sets of correlation lengths, spectral indexes, and weights for the two polarizations. However, in this paper, not to increase the number of parameters of the model, we took the weights $C^{(\sigma)}$ and the correlation lengths equal for both polarizations. Thus we will no longer specify the dependence on σ in the following, except for the polarization vectors and the random phases. The rollover wave number separates the injection range from the inertial range in the spectrum, that is, the region where the spectrum is rather flat from the region where it is represented by a power law. The correlation lengths are related to l_i ($i = x,y,z$) by the relation

$$l_{ci} = \min(2\pi l_i, \lambda_i^{\max}), \qquad (4)$$

where $\lambda_i^{\max}$ is the maximum wavelength in the ith direction (see Ref. [15]). We enforce the reality of $\delta\mathbf{B}(\mathbf{r})$ by setting $\delta B^{(\sigma)}(-\mathbf{k}) = \delta B^{(\sigma)}(\mathbf{k})$ and $\phi_{-\mathbf{k}}^{(\sigma)} = -\phi_{\mathbf{k}}^{(\sigma)}$. The above magnetic fluctuation model allows us to represent a wide class of relevant physical situations for magnetic turbulence. By varying l_i, either a pure power law or white noise can be

obtained, while anisotropy is introduced in a simple way by choosing different l_x, l_y, and l_z. For instance, the well known 2D turbulence can be obtained taking the limit $l_{c\parallel}/l_{c\perp}\to\infty$ of 3D turbulence [here $l_{c\parallel}=l_{cz}$ and $l_{c\perp}=\sqrt{(l_{cx}^2+l_{cy}^2)/2}$], and setting the weight of the magnetosonic polarization to zero, $C^{(2)}\equiv 0$, while the so-called slab model [14,18] is obtained in the limit $l_{c\parallel}/l_{c\perp}\to 0$. As shown in Ref. [23], by choosing different parameters for the two polarizations, the model can adequately describe the solar wind magnetic turbulence.

Rather than using a cubic simulation box, we expand the simulation box in the directions where the correlation lengths are larger, in the same proportion as the lengths l_i. In other words, the periodic box will be dilated by a factor l_i in the ith direction. This leads to considering the wave numbers in the following way:

$$\mathbf{k}=2\pi\left(\frac{n_x}{l_x},\frac{n_y}{l_y},\frac{n_z}{l_z}\right), \tag{5}$$

where the harmonic numbers n_i are integers. The spectrum has a ''high frequency'' cutoff when

$$k_x^2l_x^2+k_y^2l_y^2+k_z^2l_z^2>4\pi^2N^2, \tag{6}$$

where N is the maximum harmonic number. This is related to the extension of the spectrum and its value is fixed by the available numerical resources. In this way, the spectrum in $\mathbf{k}$ space has the shape of an ellipsoid, with axes proportional to $1/l_i$. In a numerical realization of turbulence only a discrete number of modes can be represented. This can introduce unwanted effects, such as dominance of a few modes of long wavelength. As shown in Ref. [15], those effects, as well as the influence of periodicity of the numerical model, are effectively reduced with the use of a *band* spectrum, where a long wavelength cutoff is introduced by taking away the modes with

$$k_x^2l_x^2+k_y^2l_y^2+k_z^2l_z^2<4\pi^2N_{\min}^2. \tag{7}$$

The void around the center also has the shape of an ellipsoid, and we note that the number of wave vectors is the same along each axis. To have many wave vectors also along the ''short'' axis is essential to have a good discretization of anisotropic turbulence.

Looking at Eq. (4), we find that the correlation lengths are proportional either to the parameters l_i or to the maximum wave lengths $\lambda_i^{\max}$, and Eq. (5) shows that $\lambda_i^{\max}$ is also proportional to l_i. Then a particular anisotropy in the spectrum can be represented by choosing, for the parameters l_i, values proportional to the correlation lengths.

To trace the magnetic field lines we integrate the equation

$$\frac{d\mathbf{r}}{ds}=\frac{\mathbf{B}(\mathbf{r})}{|\mathbf{B}(\mathbf{r})|}, \tag{8}$$

where s is the field line length. In order to save computer time, we introduce a 3D lattice with $8N$ points in each direction, on which the magnetic field components are computed exactly. Then, when integrating, the magnetic field is obtained by quadratic interpolation on this grid. We checked that eight points per minimum wavelength are enough to obtain satisfactory precision (see Ref. [15]). In this way we obtain the same number of grid points in all directions, with the density of grid points proportional to the field gradients in each direction. Typically the value of N is set to 14, while $N_{\min}=\sqrt{17}$. For all the numerical runs we set $\gamma=3/2$, which is a typical value of the spectral index in the inertial range of the MHD turbulence.

TABLE I. Parameters of the different runs of numerical simulations.

Run	l_x/l_y	$\langle\delta B_y^2\rangle/\langle\delta B_x^2\rangle$	$\langle\delta B_z^2\rangle/\langle\delta B_x^2\rangle$
1	1	1.059	1.037
2	2	0.705	0.710
3	3	0.615	0.622
4	5	0.550	0.558
5	8	0.520	0.529
6	10	0.513	0.520

The magnetic fluctuations are normalized by setting

$$\frac{\delta B}{B_0}=\sqrt{\frac{\Sigma_{ijk}\delta B_{ijk}^2\Delta V}{l_xl_yl_zB_0^2}}, \tag{9}$$

where $\delta B/B_0$ is the desired fluctuation level, and $\Delta V=l_xl_yl_z/(8N)^3$ is the volume of the cell in the grid, and where the sum is made all over the grid points.

B. Choice of correlation lengths

Of the three parameters l_x, l_y, and l_z, only two are independent, as far as the modeling of the anisotropy is concerned. One can describe the anisotropy with the ratios l_x/l_y and l_y/l_z, keeping l_z fixed (although varying the value of l_z could be used to shift the wave modes from the initial range to the injection zone of the spectrum [15]). In this paper, we fix $l_z=L$, where L is the unit length. Clearly, a complete exploration of the parameter space l_x/l_y and l_y/l_z would require large computer time, and would make the presentation of the numerical results unwieldy (every case is also studied as a function of $\delta B/B_0$). Therefore, in this paper we refer to the anisotropy found in the solar wind magnetic turbulence. Carbone, Malara, and Veltri [23] obtained different sets of correlation lengths that depend both on the two polarizations and on the distance from the Sun. However the main result of the analysis of those authors is the very high value of l_x compared to l_y and l_z, for both polarizations; this means that almost all waves vectors lay in the plane containing the average magnetic field and the solar wind velocity. Therefore the anisotropy is very strong in the xy plane, that is, in the plane perpendicular to $\mathbf{B}_0$ where transport is to be considered. For the sake of simplicity, we keep the weight of both polarizations ($C^{(1)}=C^{(2)}$) equal, and in order to understand what are the effects of the anisotropy we progressively increase the value l_x/l_y, with $l_y/l_z=1$ fixed. With such choices, the wave modes are always in the power-law part of the spectrum. The values of l_x/l_y for the various runs are listed in Table I. The ratios $\langle\delta B_y^2\rangle/\langle\delta B_x^2\rangle$ and $\langle\delta B_z^2\rangle/\langle\delta B_x^2\rangle$, also listed in Table I, give the distribution of magnetic en-

ergy for each direction, and are therefore a measure of anisotropy of the simulated magnetic field. As can be seen, the magnetic energy along x is the largest, as in the solar wind [23].

III. NUMERICAL RESULTS

For each run listed in Table I, we did two kinds of studies. First, in order to obtain a qualitative overview of transport and of the structure of the magnetic field, we drew the Poincaré sections. Second, we did a quantitative study by calculating the mean square displacements $\langle \Delta x_i^2 \rangle$ as a function of s. In both cases the starting point of each field line is taken at $z=0$ and randomly distributed in the rectangle $0 \leqslant x \leqslant l_x$, $0 \leqslant y \leqslant l_y$, in order to explore the entire area of the simulation box where the magnetic field perturbations are set up. In each case, this was done for different fluctuation levels $\delta B/B_0$.

A. Poincaré sections

The Poincaré sections are obtained by plotting in the plane xy the field line coordinates for each integer value of z/l_z. We follow a few field lines (typically 12 lines), integrating Eq. (8) from $s=0$ to $s=600 l_z$. Since the Lévy flights are found in the stochastic layer in between the closed magnetic surfaces [33], and since this layer corresponds to the percolation layer [5], we will assume that the percolating field lines which are seen on the Poincaré sections are an indication of superdiffusion. We can observe the different regimes already seen in the isotropic case [15]: for low values of the fluctuation level, we find closed curves which correspond to good magnetic surfaces, i.e., to *KAM* tori, and there are also some field lines travelling in the stochastic layer without forming a closed magnetic surface (percolating field lines), indicating that we may have enhanced diffusion. As $\delta B/B_0$ increases, we obtain the usual patterns where the magnetic surfaces are progressively destroyed until a globally stochastic regime is reached (see Fig. 1). Figure 1 is obtained with $l_x/l_y=8$, and the elongation of the magnetic islands in the x direction is evident. Figure 2 shows the Poincaré sections for l_x/l_y, growing from 2 to 5 to 10 at constant $\delta B/B_0=0.4$. It is clear that the magnetic surfaces become more elongated in x with the increase of l_x/l_y. Also, the pace of transport is reduced with the increase of the anisotropy (note the values on the x and y axes).

In the anisotropic case, one cannot immediately evaluate from the Poincaré sections whether transport is anisotropic or not, since the starting point of the magnetic field lines are not injected in a square, but in a rectangle $l_x \times l_y$. However, we note that for the lower fluctuation levels, some magnetic field lines are going from a magnetic island to another island, i.e., some percolating field lines are found. We note that by adopting a *band* spectrum with a long wavelength cutoff at about $l_i/4$, the typical island size is $\sim \frac{1}{4}$ of l_i; therefore, the motion of a field line from an island to the next is not due to periodicity, but to the percolation of magnetic surfaces [5,33]. This percolation clearly appears to be prevalent in the y direction [see panels (a) and (b) of Fig. 1]: we see that many lines pass among the islands in this direction in spite of the fact that the correlation length is smaller than that in the

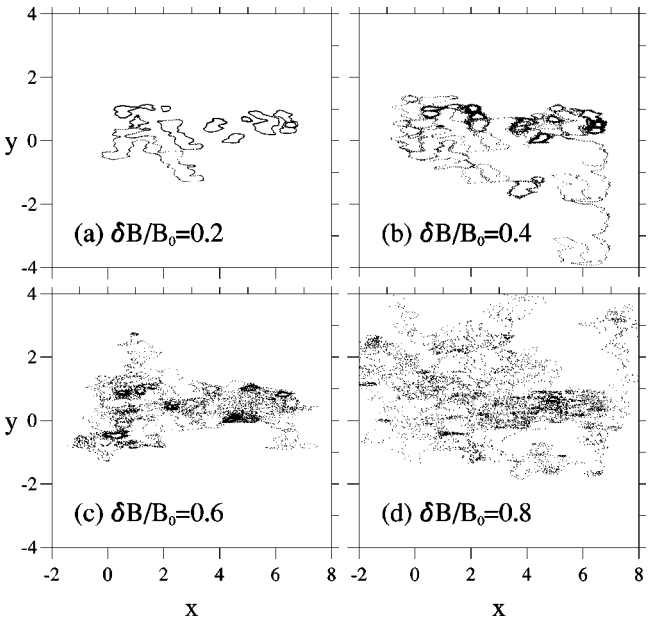

FIG. 1. Poincaré sections for run 5 ($l_x/l_y=8$) at various fluctuation levels: (a) $\delta B/B_0=0.2$. (b) $\delta B/B_0=0.4$. (c) $\delta B/B_0=0.6$. (d) $\delta B/B_0=0.8$. Dimensionless units.

x direction. It appears that the anisotropy gives a particular structure to the magnetic field percolation. The magnetic islands, because of the anisotropy in the correlation lengths, are stretched in the x direction, and the distance between the magnetic islands is also stretched in the same way, i.e., elongated in the x direction and shortened in the y direction. We

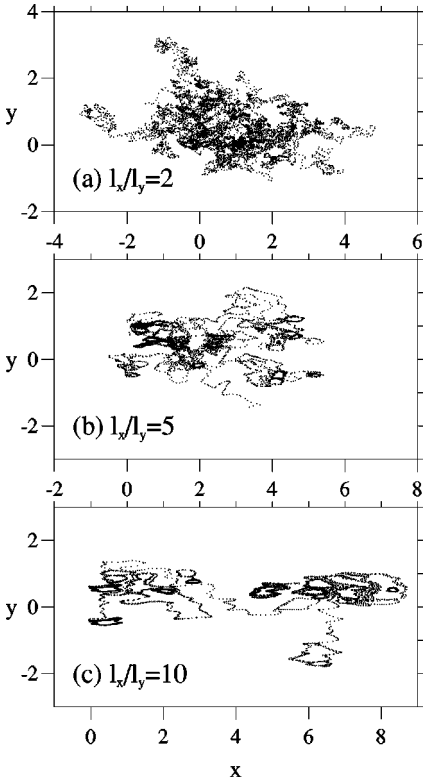

FIG. 2. Poincaré sections at $\delta B/B_0=0.4$ for various anisotropy l_x/l_y: (a) $l_x/l_y=2$. (b) $l_x/l_y=5$. (c) $l_x/l_y=10$. Dimensionless units.

argue that a magnetic field line approaching a hyperbolic point in the stochastic layer may have more chances to pass beyond the hyperbolic point across the direction where the distance between two islands is larger (the x direction), and so travel along the y direction. In addition, the gradient of the magnetic fluctuations is larger in the y direction, so that the instability of trajectories is stronger in this direction too. This is suggested by the Poincaré sections, since we observe Lévy flights mostly in the y direction (see Figs. 1 and 2), and is confirmed by the analysis of transport reported in the following.

We can notice an important feature on Fig. 2: when the anisotropy l_x/l_y is increased, the stochastic regime where the magnetic islands in the Poincaré sections are completely destroyed (which, broadly speaking, corresponds to Gaussian diffusion; see below), is reached for a higher level of fluctuations $\delta B/B_0$. It is clear from these figures that anisotropy reduces the level of stochasticity. This can be understood in the following way: by increasing the anisotropy, we squeezed the volume in **k** space in one direction, and in this way approached a 2D turbulence. Indeed, increasing any of l_i in Eq. (3) reduces the amplitude and extension in **k** space of the wave vectors in the ith direction. It appears that the smaller the size of the turbulence in **k** space, the less the stochasticity. This agrees with the results of Ref. [12], whose authors showed that increasing the extent of the 3D turbulence spectrum corresponds to an increase of stochasticity, at a fixed fluctuation level. Also, it is well known that the field line equations for strictly 2D turbulence in the plane perpendicular to $\mathbf{B_0}$ are not chaotic, corresponding to a one-degree-of-freedom Hamiltonian, and increasing l_x squeezes the value of excited wave vectors toward a 2D domain. Moreover, it was shown analytically that one-dimensional fluctuations $\delta B_x(y,z)$ can give rise to chaotic field line evolution if, and only if, shear is introduced into the average field configuration, that is, if $\mathbf{B}_0 = B_0(\hat{e}_z + (x/L)\hat{e}_y)$ [3,4,34]. Therefore, not only the extension in **k** space, but also the dimensionality of the magnetic field variations, is important in determining the level of stochasticity. This fact can also be appreciated with a naïve reduction of our magnetic turbulence model. Let us consider a simple three wave magnetic field model, similar to the Arnold-Beltrami-Childress flow:

$$\delta B_x = a\ \sin(2\pi y) + b\ \sin(2\pi z),$$

$$\delta B_y = \epsilon\ \cos(2\pi x) + b\ \cos(2\pi z), \tag{10}$$

$$B_z = \epsilon\ \cos(2\pi x) + a\ \sin(2\pi y) + B_0,$$

where a, b, and ϵ are constants. This magnetic field model is isotropic in the (x,y) plane when $a=b=\epsilon$, that is the energy density in the x direction, $\langle \delta B_x^2 \rangle$, is the same as that in the y direction, $\langle \delta B_y^2 \rangle$. The parameter ϵ is the amplitude of the wave mode depending on x, and decreasing ϵ corresponds to increasing l_x in Eq. (3): in this way, the perturbations along the axes are ''anisotropic,'' and the energy density $\langle \delta B_x^2 \rangle$ is the largest, as in the present turbulence model. The Poincaré sections obtained numerically are shown in Fig. 3 for $a=b=0.3B_0$, and for different values of ϵ. We note in this figure that as ϵ is reduced, the magnetic islands become more elongated in x and the Poincaré sections are more ordered: we increase the anisotropy and progressively lose the stochasticity of the system. The decrease of ϵ corresponds to reducing the dimensionality of the perturbations from 3 to 2. We obtain the same effect in our model when we increase the anisotropy in the correlation lengths: we have less stochasticity as l_x/l_y is increased. We note that this reduction of stochasticity is even stronger if both l_x/l_y and l_y/l_z are increased, as shown by other runs which are not presented in detail in this paper.

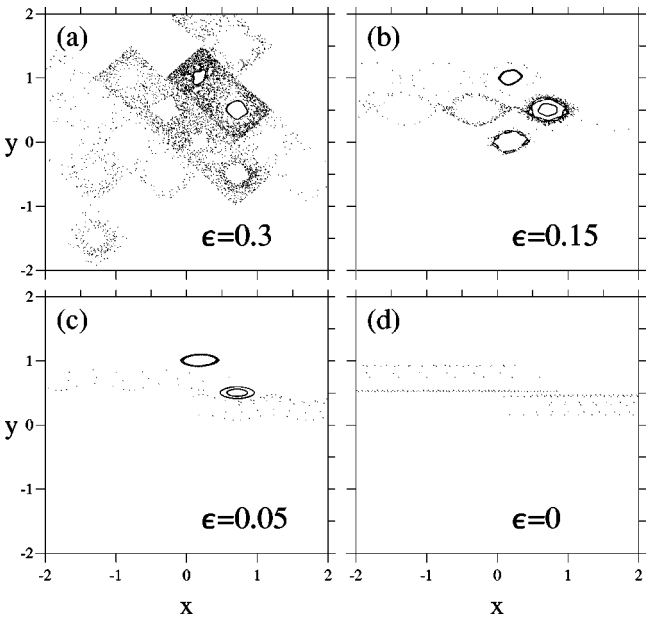

FIG. 3. Poincaré sections for a three wave magnetic model where the perturbation depending on x is reduced progressively to 0. (a) $\epsilon=0.3$. (b) $\epsilon=0.15$. (c) $\epsilon=0.05$. (d) $\epsilon=0.0$. Dimensionless units.

B. Transport properties

For each case listed in Table I, we did an accurate quantitative study, by calculating $\langle \Delta x_i^2 \rangle$ as a function of s, averaged over 1000 field lines and for s going up to 1000–1500 L. In all cases the starting point $\mathbf{r}_0$ of each field line is taken at $z=0$ and randomly distributed in the rectangle $0 \leqslant x \leqslant l_x$, $0 \leqslant y \leqslant l_y$. In order to evaluate the displacement from the initial position of every field line, we consider $\Delta x = x - x_0$ and $\Delta y = y - y_0$. In this way the transport results do not depend on the fact that when $l_x > l_y$ the bundle of field lines is larger in the x direction than in the y direction at $z=0$, so that the corresponding spread $\langle (x - \langle x \rangle)^2 \rangle$ would be larger than $\langle (y - \langle y \rangle)^2 \rangle$ from the start. In other words, we eliminate the anisotropy due to the injection scheme. We made a fit of the computed $\langle \Delta x_i^2 \rangle(s)$, with the transport law

$$\langle \Delta x_i^2 \rangle = 2D_i s^{\alpha_i}, \quad i=(x,y) \tag{11}$$

and determined α_i and D_i when s is large enough to attain asymptotic values.

In Fig. 4 we report the anomalous diffusion exponents α_i for runs 1–6. We find a distinct behavior of the transport as a function of the fluctuation level: for lower fluctuation levels we have either a subdiffusive regime where $\alpha<1$, or sometimes a superdiffusive regime, $\alpha>1$. Then, at a particu-

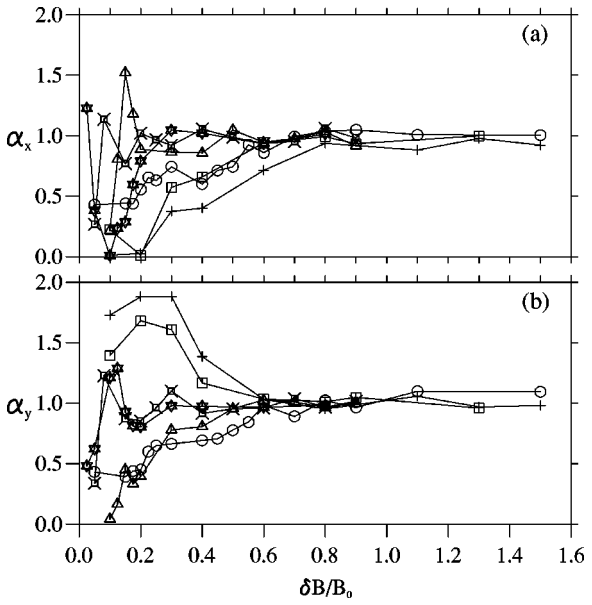

FIG. 4. Exponent α for the direction x and y vs fluctuation level $\delta B/B_0$. Sun: $l_x/l_y=1$; star: $l_x/l_y=2$; triangle: $l_x/l_y=3$; circle: $l_x/l_y=5$; square: $l_x/l_y=8$; cross: $l_x/l_y=10$. Dimensionless units.

lar fluctuation level $(\delta B/B_0)^*$, which appears to increase with the level of anisotropy, as suggested by the analysis of the Poincaré sections, normal diffusion is reached in both directions ($\alpha \approx 1$). In order to reach the Gaussian regime for the cases with high anisotropy, it was necessary to set $\delta B/B_0 \gtrsim 1$. On the one hand, this shows how strong the effect of anisotropy is; on the other hand, such high fluctuation levels are sometimes but not often found for MHD turbulence in the solar wind. Thus different transport regimes could be found in the different cases.

The diffusion coefficients D_x and D_y are reported in Fig. 5 for all the runs when $\alpha_x, \alpha_y \simeq 1$. Starting from run 1 (Sun), when diffusion is isotropic and $D_x \approx D_y$, we note clearly that

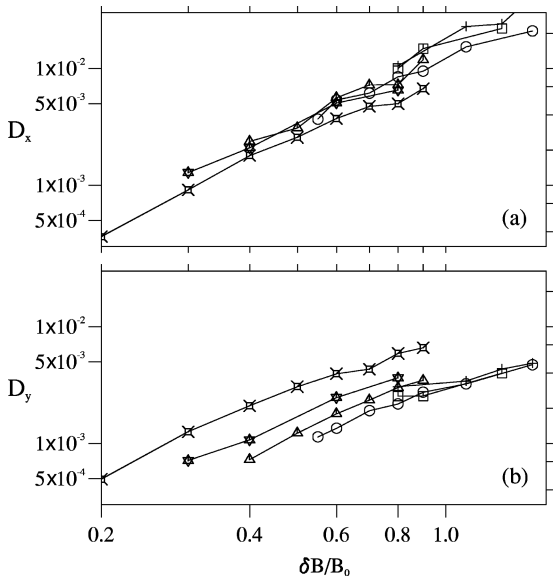

FIG. 5. The diffusion coefficients D_x and D_y (along x and y), for the different runs vs fluctuation level $\delta B/B_0$ (Same symbols as in Fig. 4). Dimensionless units.

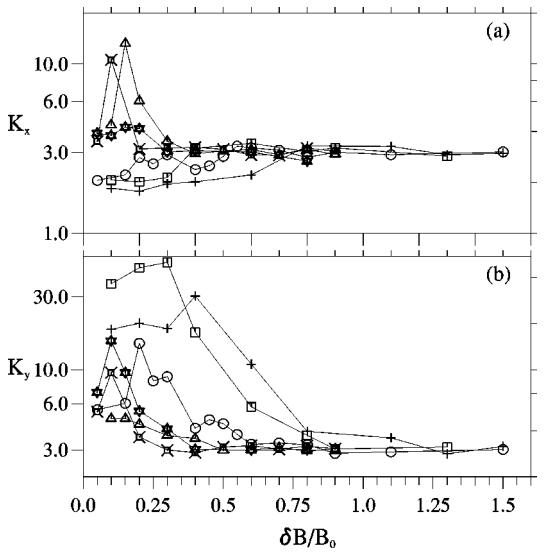

FIG. 6. Kurtosis K_x and K_y (along x and y), for the different runs vs fluctuation level $\delta B/B_0$ (Same symbols as in Fig. 4). Dimensionless units.

when increasing l_x/l_y, D_x is increasing and D_y is decreasing. Thus, in the diffusive regime, transport is enhanced in the direction where the correlation length is larger. By evaluating the slope of D_x and D_y versus $\delta B/B_0$, we obtain values very close to 2, that is we recover the quasilinear scaling. This agrees with the results of Refs. [12,14].

From the integrated field lines, the kurtosis $K_i = \langle (\Delta x_i)^4 \rangle / \langle (\Delta x_i)^2 \rangle^2$, $i=x,y$, is easily obtained (Fig. 6). When the distribution function of field lines is Gaussian, the kurtosis is equal to 3, and, when it is larger than 3, the tails of the distribution are more important than in the Gaussian case. This is clearly the case for Lévy random walk, since the tails of the limit distribution of probability are power laws, so that the tails are very important [12,15]. Indeed by looking at K_x and K_y in Fig. 6, we note that for the low fluctuation levels we are not in Gaussian regime. Further, the value of $\delta B/B_0$ for which the kurtosis is close to 3 is increasing with the anisotropy l_x/l_y. In general, the kurtosis approaches 3 when normal diffusion is attained. By comparing Figs. 4 and 6, we can see that, for the x direction, $\alpha_x < 1$ corresponds to $K_x < 3$ and $\alpha_x > 1$ corresponds to $K_x > 3$, as already found in the isotropic cases [12,15]. On the other hand, for the y direction, we find a value of K_y substantially larger than 3 even in cases of subdiffusion, $\alpha_y < 1$, in particular for run 4 ($l_x/l_y=5$). This means that even if the global spread of the bundle of field lines $\langle \Delta y^2 \rangle$ grows slower than linearly with arc length s, the distribution of field line positions in y has longer tails than a Gaussian. This is due to the fact, as already pointed out, that field lines easily percolate along y: in many cases percolation is not strong enough to give rise to superdiffusion, but it is sufficient to cause a departure from a Gaussian distribution for field line positions. In this connection, we note that the Lévy flight statistical models involve power-law distributions for the jump lengths with diverging second order moment even in cases of subdiffusion [35]. In Fig. 7 we plot the value of $(\delta B/B_0)^*$ for which the kurtosis attains 3.0 ± 0.3 versus the anisotropy ratio l_x/l_y, and this plot shows a net increase of $(\delta B/B_0)^*$ with the anisotropy. In general, it unambiguously appears that the increase of

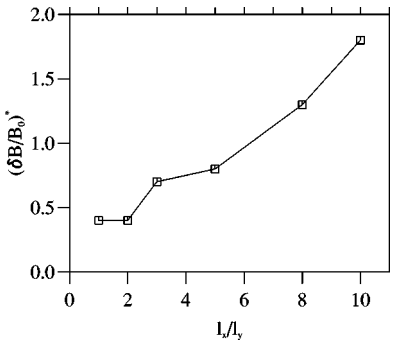

FIG. 7. Minimum value of the fluctuation level $(\delta B/B_0)^*$ at which the kurtosis is between 3.3 and 2.7, as a function of the ratio l_x/l_y. Dimensionless units.

anisotropy decreases the level of stochasticity and retards the reach of the Gaussian regime. In other words, the increase of anisotropy works in the opposite way than the extension of the spectrum. Indeed, in a previous paper, using the same numerical technique but in the isotropic case, Zimbardo *et al.* [12] found that by increasing the volume in phase space, i.e., by increasing the extension of the spectrum, global stochasticity was obtained for a decreasing level of fluctuations $\delta B/B_0$ (a well known result).

1. Influence of level of anisotropy l_x/l_y on the superdiffusive regime

Although for many cases at low values of $\delta B/B_0$ we are in the subdiffusive regime, particularly in the x direction, we find $\alpha_y > 1$ for different cases in the y direction (see Fig. 4), meaning that the transport regime is not Gaussian but is superdiffusive with the occurrence of Lévy flights. As indicated by the Poincaré sections, superdiffusion and Lévy flights occur mainly in the y direction, that is, in the direction where the correlation length (in the xy plane) is shorter. This is rather surprising since Lévy flights are due to long correlation in the random walk [33,36,37]. This result can be understood by noting the following: the ''elementary'' displacements along x are longer than those along y by the ratio l_x/l_y, which corresponds to the elongation of the magnetic islands, but the displacements along y are long range correlated because of the above mentioned tendency to cross the hyperbolic points along the y directions. It is the long range correlation of the steps of the random walk that gives rise to superdiffusion, irrespective of the length, proportional either to l_x or to l_y, of the steps.

We find superdiffusion for the two runs with the lowest anisotropy l_x/l_y (runs 1 and 2), while, for runs 3 and 4, there is no superdiffusion. We note from Fig. 4 that superdiffusion is less important for runs 1 and 2, where α_x and α_y attain a maximum value of 1.3, than for runs 5 and 6, where $\alpha_y > 1.5$. We argue that the superdiffusion obtained for runs 1 and 2 is a residual effect of isotropic superdiffusion, and indeed both $\alpha_x > 1$ and $\alpha_y > 1$ [15]. Then, for run 4, where both α_x and $\alpha_y \lesssim 1$, we are in a transition regime between isotropic superdiffusion and anisotropic superdiffusion. Finally, increasing the anisotropy l_x/l_y (see runs 5 and 6 in Fig. 4) sufficiently, we obtain reinforced Lévy flights along y which confirm the possibility of superdiffusion along the direction where the correlation length is the smaller.

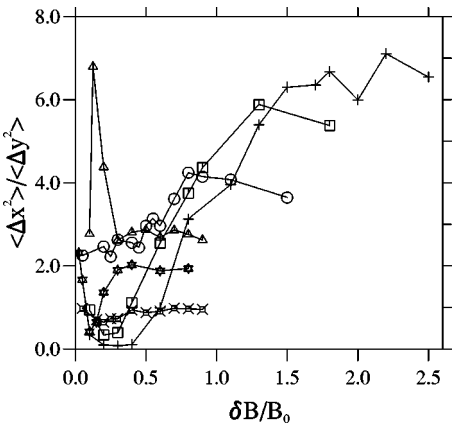

FIG. 8. Ratio $\langle \Delta x^2 \rangle / \langle \Delta y^2 \rangle$ (averaged for $s = 800-1000$) vs fluctuation level (Same symbols as in Fig. 4). Dimensionless units.

2. Influence of level of anisotropy l_x/l_y on transport in the diffusive regime

For the physical application it is of prime importance to understand what is the anisotropy of transport in anisotropic turbulence. Thus in Fig. 8 we plot the ratio of mean square displacements $\langle \Delta x^2 \rangle / \langle \Delta y^2 \rangle$ averaged from $s = 800$ to 1000, i.e., in the asymptotic regime, versus $\delta B/B_0$, and for different values of the anisotropy l_x/l_y. This ratio gives a global idea of the anisotropy of transport, since, as discussed earlier, the calculation of the mean square displacement does not depend on the fact that the box is longer in the x direction. Figure 8 presents several interesting features: when the Gaussian regime is attained, $\langle \Delta x^2 \rangle / \langle \Delta y^2 \rangle$ tends to an asymptotic value $(\langle \Delta x^2 \rangle / \langle \Delta y^2 \rangle)^*$. This ratio increases when the level of anisotropy is increased, and we have that $(\langle \Delta x^2 \rangle / \langle \Delta y^2 \rangle)^* \sim D_x/D_y \sim l_x/l_y$. Figure 9 shows the ratio D_x/D_y versus l_x/l_y; analyzing Fig. 9, we find the following trend: $D_x/D_y \sim (l_x/l_y)^{13/14}$, that is, an almost linear dependence.

This shows that the ratio $\langle \Delta x^2 \rangle / \langle \Delta y^2 \rangle$ depends directly on the anisotropy in the plane perpendicular to the direction of the magnetic field. A rather anisotropic situation, such as we expect in the solar wind, $l_{cx}/l_{cy} \gg 1$, can then lead to much faster diffusion in the x direction than in the y direction, and thus enhance magnetic field line transport in the heliographic latitude (clearly we expect that such picture applies if the fluctuation level of the solar wind turbulence is strong enough to obtain a diffusive behavior).

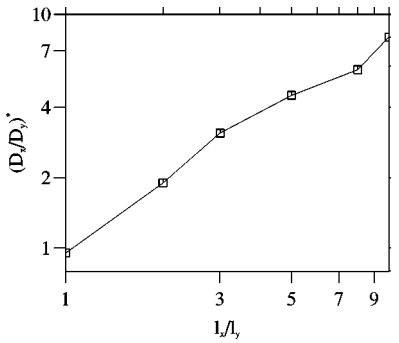

FIG. 9. Ratio $(D_x/D_y)^*$, when the Gaussian regime is attained, vs level of anisotropy l_x/l_y. Dimensionless units.

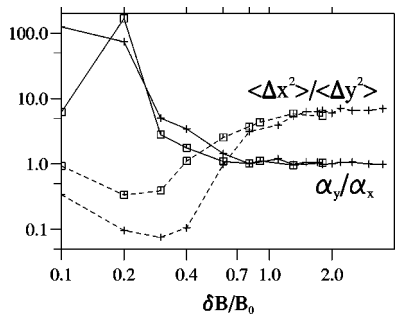

FIG. 10. The superdiffusion along the y direction for a lower fluctuation level, and the Gaussian regime of diffusion prevalent in the x direction when $\delta B/B_0$ is increased, is shown by the ratio $\langle \Delta x^2 \rangle / \langle \Delta y^2 \rangle$ (dashed line) and α_y/α_x for runs 5 and 6 (full line). Dimensionless units.

We note that $\langle \Delta x^2 \rangle / \langle \Delta y^2 \rangle$ changes from smaller than 1 in the Lévy flights regime to larger than 1 in the Gaussian regime. This inversion is better illustrated for runs 5 and 6 in Fig. 10, where the values of $\langle \Delta x^2 \rangle / \langle \Delta y^2 \rangle$ and α_y/α_x are plotted for these two runs at different $\delta B/B_0$. This inversion was unexpected, as was the superdiffusion along y, and this means that in order to assess the effects of anisotropic turbulence on the anisotropy of transport it is fundamental to know whether the system is in an anomalous transport regime or in a Gaussian globally stochastic regime.

IV. DISCUSSION AND CONCLUSIONS

In this paper a numerical study of magnetic field line transport in anisotropic turbulence has been carried out. The anisotropy of turbulence is introduced by varying the correlation lengths l_{cx}, l_{cy}, and l_{cz}, which appear in the Fourier amplitude. Particular care was taken in the numerical model to avoid the dominance of a few modes and the periodicity effects, by choosing a *band* spectrum, that is, introducing both short and long wavelength cutoffs. In order to have a well discretized representation of continuous turbulence, a high number of wave vectors is taken into account for each direction. This study has shown that a very rich variety of transport behaviors can be found by varying the degree of anisotropy l_{cx}/l_{cy} in the plane perpendicular to the average magnetic field. The main results are the following: (1) We find anomalous transport regimes at low fluctuation levels, and a Gaussian diffusive regime in the presence of high fluctuation levels, as in the isotropic case. (2) As anisotropy is increased the diffusive regime is attained for higher fluctuation levels. (3) We find a percolative regime at a lower fluctuation level in the direction where the correlation length is smaller, for significant degrees of anisotropy l_{cx}/l_{cy}. (4) In the diffusive regime there is more diffusion in the direction of the longer correlation lengths, and we obtain that the ratio of diffusion coefficients D_x/D_y is close to the ratio of anisotropy l_{cx}/l_{cy}.

This numerical work shows that stochasticity is reduced when anisotropy is increased, so that the 3D domain of excited wave vectors in $\mathbf{k}$ space is reduced to an almost 2D domain. On the other hand, previous analytical work showed that the lower the dimensionality of the average field, the lower the level of stochasticity [3,4,34]. Therefore, we can conclude that the diffusive regime is reached earlier the larger the extension and dimensionality of the magnetic field variations.

The numerical results show that the anisotropy of the correlation lengths plays a very important role in the diffusion of the magnetic field line. In particular, Gaussian diffusion is faster along the direction with the larger correlation length x, while anomalous diffusion is faster along the direction with the shorter correlation length y. We ascribe this peculiar behavior to the fact that when many magnetic surfaces are forming *KAM* tori, the field lines in the stochastic layer cross the hyperbolic point region preferentially moving along y, both because the ''road'' is wider in y and because the instability of trajectories is stronger in y. Therefore, for each physical system of interest one has to understand whether the system is or is not in the diffusive regime.

When applying the above results to energetic particle transport in the solar wind, we are faced with the following puzzle: the transport regime changes from anomalous to Gaussian, increasing the fluctuation level beyond $(\delta B/B_0)^*$. However, $(\delta B/B_0)^*$ increases with the degree of anisotropy l_x/l_y, and presumably decreases with the extension of the turbulence spectrum [12]. In the solar wind the anisotropy is rather strong, $l_x \gg l_y$, which would increase $(\delta B/B_0)^*$, but the turbulence spectrum is also very long, encompassing at least three decades in the so called inertial range, which would decrease $(\delta B/B_0)^*$. However, at present it is not possible to simulate a 3D spectrum with extension $N \sim 1000$. As a consequence, we cannot determine whether the transport regime in the solar wind would be either anomalous or Gaussian. Therefore, applications of the present results to particle transport in the solar wind has to be maintained at a speculative level. If in the solar wind the extension of the spectrum is sufficient to reach the diffusive regime in the range of fluctuation levels typical of the solar wind, $\delta B/B_0 \sim 0.5-1.0$, as we believe, transport along x is faster than transport along y, and the ratio $\langle \Delta x^2 \rangle / \langle \Delta y^2 \rangle$ is close to l_x/l_y. Since in our study the x direction is normal to the $\mathbf{B}_{\mathrm{IMF}}$-$\mathbf{V}_{\mathrm{SW}}$ plane, we can conclude that translatitudinal transport is several times faster than translongitudinal transport: the implications of these results on energetic particles propagation will be considered in a future paper.

ACKNOWLEDGMENTS

This work is part of a research program which is financially supported by the Ministero dell'Università e della Ricerca Scientifica e Tecnologica (MURST), the Consiglio Nazionale delle Ricerche (CNR), Contract No. 98.00148.CT02, and the Agenzia Spaziale Italiana (ASI), Contract No. ARS98-82.

[1] M. N. Rosenbluth, R. Z. Sagdeev, G. B. Taylor, and G. M. Zaslavsky, Nucl. Fusion **6**, 297 (1966).
[2] N. N. Filonenko, R. Z. Sagdeev, and G. M. Zaslavsky, Nucl. Fusion **7**, 253 (1967).
[3] A. B. Rechester and M. N. Rosenbluth, Phys. Rev. Lett. **40**, 38 (1978).
[4] J. A. Krommes, C. Oberman, and R. G. Kleva, J. Plasma Phys. **30**, 11 (1983).
[5] M. B. Isichenko, Plasma Phys. Controlled Fusion **33**, 809 (1991).
[6] J. R. Jokipii, Astrophys. J. **146**, 480 (1966).
[7] J. R. Jokipii and E. N. Parker, Phys. Rev. Lett. **21**, 44 (1968).
[8] J. R. Jokipii and E. N. Parker, Astrophys. J. **155**, 777 (1969).
[9] E. Corbelli and P. Veltri, Astrophys. J. **340**, 679 (1989).
[10] M. M. Kuznetsova and L. M. Zelenyi, in *Physics of Magnetic Flux Ropes*, edited by C. T. Russell, Geophysical Monograph Series Vol. 58 (American Geophysical Union, Washington, D.C., 1990), p. 473.
[11] J. Giacalone and J. R. Jokipii, Astrophys. J. **430**, L137 (1994).
[12] G. Zimbardo, P. Veltri, G. Basile, and S. Principato, Phys. Plasmas **2**, 2653 (1995).
[13] G. Zimbardo and P. Veltri, Geophys. Res. Lett. **23**, 793 (1996).
[14] P. C. Gray, D. H. Pontius, Jr., and W. H. Matthaeus, Geophys. Res. Lett. **23**, 965 (1996).
[15] P. Pommois, G. Zimbardo, and P. Veltri, Phys. Plasmas **5**, 1288 (1998).
[16] P. Veltri, G. Zimbardo, and P. Pommois, Adv. Space Res. **22**, 55 (1998).
[17] M. B. Isichenko, Rev. Mod. Phys. **64**, 961 (1992).
[18] W. H. Matthaeus, P. C. Gray, D. H. Pontius, Jr., and J. W. Bieber, Phys. Rev. Lett. **75**, 2136 (1995).
[19] H. D. Wang, M. Vlad, E. Vanden Eijnden, F. Spineanu, J. H. Misguich, and R. Balescu, Phys. Rev. E **51**, 4844 (1995).
[20] J.-D. Reuss and J. H. Misguich, Phys. Rev. E **54**, 1857 (1996).
[21] M. Dobrowolny, A. Mangeney, and P. Veltri, Astron. Astrophys. **83**, 26 (1980).
[22] W. H. Matthaeus, M. L. Goldstein, and D. A. Robert, J. Geophys. Res. **95**, 20 673 (1990).
[23] V. Carbone, F. Malara, and P. Veltri, J. Geophys. Res. **100**, 1763 (1995).
[24] B. Bavassano, M. Dobrowolny, G. Fanfoni, F. Mariani, and N. F. Ness, Sol. Phys. **78**, 373 (1982).
[25] D. C. Robinson and M. G. Rusbridge, Phys. Fluids **14**, 2499 (1971).
[26] P. Veltri, G. Zimbardo, A. L. Taktakishvili, and L. M. Zelenyi, J. Geophys. Res. **103**, 14 879 (1998).
[27] C.-Y. Tu, E. Marsch, and K. M. Thieme, J. Geophys. Res. **94**, 11 739 (1989).
[28] M. Dobrowolny, A. Mangeney, and P. Veltri, Phys. Rev. Lett. **45**, 144 (1980).
[29] J. V. Shebalin, W. H. Matthaeus, and D. Montgomery, J. Plasma Phys. **29**, 525 (1983).
[30] R. Grappin, Phys. Fluids **29**, 2433 (1986).
[31] V. Carbone and P. Veltri, Geophys. Astrophys. Fluid Dyn. **52**, 153 (1990).
[32] R. Grappin, A. Mangeney, and M. Velli, in *Solar Wind Seven*, edited by E. Marsch and R. Schwenn (Pergamon, Oxford, 1992).
[33] G. Zimbardo and P. Veltri, Phys. Rev. E **51**, 1412 (1995).
[34] G. Zimbardo, P. Veltri, and F. Malara, J. Plasma Phys. **32**, 141 (1984).
[35] J. Klafter, A. Blumen, and M. F. Shlesinger, Phys. Rev. A **35**, 3081 (1987).
[36] J.-P. Bouchaud and A. Georges, Phys. Rep. **195**, 127 (1990).
[37] J. Klafter, M. F. Shlesinger, and G. Zumofen, Phys. Today **49** (2), 33 (1996).